AD-A086 129 PACIFIC-SIERRA RESEARCH CORP SANTA MONICA CA F/G 20/14
ELF PROPAGATION IN THE PRESENCE OF NONSTRATIFIED IONOSPHERIC DI--ETC(U)
UNCLASSIFIED JUN 80 E C FIELD, S J BAYER, B P D'AMBROSIO N00014-79-C-0452
PSR-1013 NL

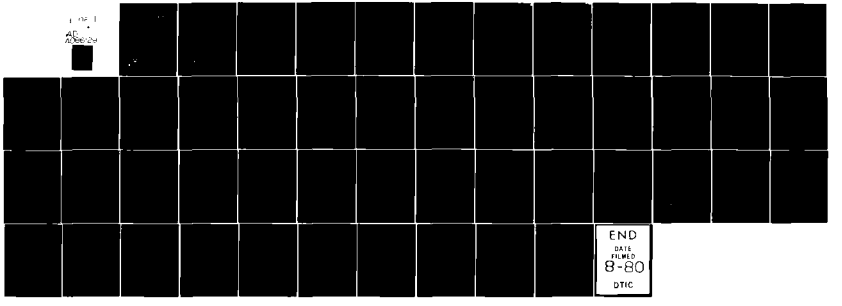

(12)

LEVEL II

PSR Report 1013

ELF PROPAGATION IN THE PRESENCE OF NONSTRATIFIED IONOSPHERIC DISTURBANCES

June 1980

E. C. Field, Jr.
S. J. Gayer
B. P. D'Ambrosio

Final Report
Contract N00014-79-C-0452

Sponsored by
Office of Naval Research
800 N. Quincy St.
Arlington, Virginia 22217

PACIFIC • SIERRA RESEARCH CORP.

PSR Report 1013

ELF PROPAGATION IN THE PRESENCE OF NONSTRATIFIED IONOSPHERIC DISTURBANCES

June 1980

E. C. Field, Jr.
S. J. Gayer
B. P. D'Ambrosio

Final Report
Contract N00014-79-C-0452

Sponsored by
Office of Naval Research
800 N. Quincy St.
Arlington, Virginia 22217

PACIFIC • SIERRA RESEARCH CORP.

SECURITY CLASSIFICATION OF THIS PAGE (When Data Entered)

REPORT DOCUMENTATION PAGE

READ INSTRUCTIONS BEFORE COMPLETING FORM

1. REPORT NUMBER: PSR ~~Report~~ 1013	2. GOVT ACCESSION NO.: AD-A056 129
3. RECIPIENT'S CATALOG NUMBER:	
4. TITLE (and Subtitle): ELF PROPAGATION IN THE PRESENCE ~~OF~~ NONSTRATIFIED IONOSPHERIC DISTURBANCES	5. TYPE OF REPORT & PERIOD COVERED: Final Report - May 1979 - February 1980
	6. PERFORMING ORG. REPORT NUMBER: PSR Report 1013
7. AUTHOR(s): E. C. Field, Jr. S. J. Gayer B. P. D'Ambrosio	8. CONTRACT OR GRANT NUMBER(s): N00014-79-C-0452
9. PERFORMING ORGANIZATION NAME AND ADDRESS: Pacific-Sierra Research Corporation 1456 Cloverfield Blvd. Santa Monica, California 90404	10. PROGRAM ELEMENT, PROJECT, TASK AREA & WORK UNIT NUMBERS: Task NR089-144
11. CONTROLLING OFFICE NAME AND ADDRESS: Office of Naval Research 800 N. Quincy St., Code 464 Arlington, Virginia 22217	12. REPORT DATE: June 1980 13. NUMBER OF PAGES: 38
14. MONITORING AGENCY NAME & ADDRESS(if different from Controlling Office)	15. SECURITY CLASS. (of this report): Unclassified 15a. DECLASSIFICATION/DOWNGRADING SCHEDULE

16. DISTRIBUTION STATEMENT (of this Report)

Approved for Public Release and Sale; Distribution Unlimited

17. DISTRIBUTION STATEMENT (of the abstract entered in Block 20, if different from Report)

18. SUPPLEMENTARY NOTES

19. KEY WORDS (Continue on reverse side if necessary and identify by block number)

ELF propagation
Submarine communications
Nuclear environments

20. ABSTRACT (Continue on reverse side if necessary and identify by block number)

This report analyzes the propagation of the TEM-ELF waveguide mode when the ionosphere is not stratified. It treats strong localized ionospheric disturbances by recasting the lateral wave equation as a two-dimensional integral equation, and applies a specially developed algorithm to obtain numerical solutions. The quasi-full-wave results show that a localized ionospheric disturbance behaves like a converging cylindrical lens filling a narrow aperture. Lateral diffraction and focusing, ignored in treatments that do not fully account for transverse ionospheric structure, cause the ELF signal to exhibit

Next page

DD FORM 1 JAN 73 1473 EDITION OF 1 NOV 65 IS OBSOLETE

SECURITY CLASSIFICATION OF THIS PAGE (When Data Entered)

BLOCK 20 (Cont.)

a pattern of maxima and minima on the line normal to the path passing through the center of the disturbance. As expected, the focusing/diffraction effects diminish when the transverse dimension of the disturbance exceeds the width of the first Fresnel zone--typically, several megameters.

The analysis models widespread inhomogeneities, such as within the polar cap or at the day/night terminator, as semiinfinite regions separated by diffuse boundaries; it then derives full-wave analytic expressions for the reflection of the TEM mode. Mode reflection is found to significantly affect an ELF signal in two actual situations: first, when receivers are on great circle paths that are nearly tangential to the disturbed polar cap--in which case shadow zones and interference patterns can occur; and second, when signals are incident on the day/night terminator (from the day side) at angles exceeding about 75 deg--in which case the signals are affected by a phenomenon analogous to total internal reflection. Reflection is found to be unimportant if the boundary thickness exceeds about one-sixth of a wavelength.

PREFACE

This report concludes Pacific-Sierra Research Corporation's (PSR's) analysis of the effects of nonstratified ionospheric disturbances on ELF propagation. It extends the treatments presented in two previous documents: *ELF Propagation in a Non-Stratified Earth Ionosphere Waveguide*, PSR Report 806, April 1978; and *An Integral Equation Approach to ELF Propagation in a Non-Stratified Earth-Ionosphere Waveguide*, PSR Report 904, February 1979. The work was sponsored by the Office of Naval Research, Arlington, Virginia.

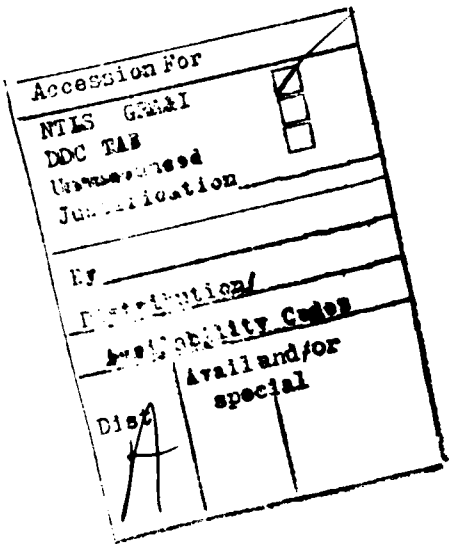

SUMMARY AND CONCLUSIONS

This report analyzes the propagation of the TEM-ELF waveguide mode when the ionosphere is not stratified. It treats strong localized ionospheric disturbances by recasting the lateral wave equation as a two-dimensional integral equation, and applies a specially developed algorithm to obtain numerical solutions. The quasi-full-wave results show that a localized ionospheric disturbance behaves like a converging cylindrical lens filling a narrow aperture. Lateral diffraction and focusing, ignored in treatments that do not fully account for transverse ionospheric structure, cause the ELF signal to exhibit a pattern of maxima and minima on the line normal to the path passing through the center of the disturbance. As expected, the focusing/diffraction effects diminish when the transverse dimension of the disturbance exceeds the width of the first Fresnel zone--typically, several megameters.

The analysis models widespread inhomogeneities, such as within the polar cap or at the day/night terminator, as semiinfinite regions separated by diffuse boundaries; it then derives full-wave analytic expressions for the reflection of the TEM mode. Mode reflection is found to significantly affect an ELF signal in two actual situations: first, when receivers are on great circle paths that are nearly tangential to the disturbed polar cap--in which case shadow zones and interference patterns can occur; and second, when signals are incident on the day/night terminator (from the day side) at angles exceeding about 75 deg--in which case the signals are affected by a phenomenon analogous to total internal reflection. Reflection is found to be unimportant if the boundary thickness exceeds about one-sixth of a wavelength.

CONTENTS

FIGURES

I. INTRODUCTION

This report treats the propagation of the transverse electromagnetic (TEM) extremely-low-frequency (ELF) waveguide mode under conditions in which the ionosphere is not stratified. We consider both widespread and laterally bounded inhomogeneities of arbitrary strength, and impose no restrictions on the direction of propagation relative to ionospheric gradients. The report therefore supplements Field and Joiner's [1979] integral-equation analysis of ELF propagation, which yielded numerical results for (1) weak, localized ionospheric disturbances remote from both transmitter and receiver, and (2) ionospheric disturbances of arbitrary strength and extent, azimuthally symmetric about the transmitter. Findings accounted, in the first case, for gradients transverse to the propagation path, and in the second case, for gradients parallel to the direction of propagation. The results also showed the relationship between the fraction of the first Fresnel zone filled by an ionospheric disturbance and the resulting propagation anomaly.

To analyze the propagation effects of widespread ionospheric inhomogeneities, the present analysis develops a computational model that assumes two laterally uniform--but vertically nonuniform--semiinfinite regions. The model is adequate to describe reflections from such wide areas as the polar cap during a solar proton event (SPE), the zone affected by a solar X-ray flare, and the day and night portions of the earth, and would also apply to the disturbance created by a nuclear burst at altitudes above a few hundred kilometers. Bounding such areas are transition regions in which the waveguide varies over a few hundred to perhaps two thousand kilometers. Since those distances compare to $\lambda/2\pi$ (where λ is wavelength), the simplifications associated with either sharp (Fresnel coefficients) or gentle (Wenzel-Kramers-Brillouin [WKB] calculations) boundaries cannot be used at ELF. We therefore use a full-wave theory that completely accounts

for the lateral diffuseness of the boundaries but still yields closed-form solutions for the reflection coefficients.*

Closed-form solutions are not possible for strong ionospheric disturbances that are too localized for approximation as semiinfinite regions. To treat the localized situation, we recast the lateral wave equation as a two-dimensional integral equation, then develop a special algorithm to obtain numerical solutions. The full-wave results account for the lateral focusing and diffraction omitted from earlier, less-exact formulations.

Section II reviews the two-dimensional wave equations that approximately describe ELF propagation in a laterally nonuniform earth-ionosphere waveguide. Section III presents models for the waveguide propagation constant in ambient and disturbed regions. Section IV adapts the Epstein theory of propagation in vertically inhomogeneous ionospheres so as to yield the lateral reflection coefficient of the TEM-ELF waveguide mode. Section V presents numerical results for several model disturbances. The Appendix describes the algorithm used to solve the two-dimensional integral-wave equation.

---

*The theory applies only to ELF, which is characterized by a single propagating waveguide mode. At higher frequencies, any boundary abrupt enough to require the full-wave theory would cause coupling among higher order modes, not accounted for here.

II. PROPAGATION IN LATERALLY NONUNIFORM EARTH-IONOSPHERE WAVEGUIDE

The wave equation can be solved by separation of variables under conditions in which the ionosphere is laterally uniform.* The result, well known from Galejs [1972], for example, is

$$E_0 = A\Lambda_0 F_0(z)\tilde{E}_0(x, y) \quad \text{V/m} , \tag{1}$$

where E_0 is the vertical component of the electric field; A is a constant involving dipole moment, wave frequency, and ground conductivity; Λ_0 is the excitation factor representing the efficiency with which the TEM waveguide mode is launched; $F_0(z)$ is the height-gain function for the vertical dependence of the field, normalized to unity at z = 0; x, y, and z are Cartesian coordinates; and the subscript 0 denotes undisturbed, laterally homogeneous conditions.

The lateral dependence of the field is governed by the function $\tilde{E}_0$, which satisfies the two-dimensional wave equation

$$\left(\nabla_T^2 + k^2 S_0^2\right)\tilde{E}_0 = 0 , \tag{2}$$

where ∇_T^2 is the two-dimensional Laplacian, k is the free-space wave number, and S_0 is a waveguide propagation constant determined by imposing boundary conditions on F_0 at the ground and in the ionosphere. The literature supplies full-wave methods for calculating S_0 and Λ_0 for virtually any ionospheric height profile, as well as numerical results for many models of ambient and disturbed ionospheres [Budden, 1961; Field, 1970; Wait, 1970; Galejs, 1972; Pappert and Moler, 1974; Greifinger and Griefinger, 1978]. Once S_0 is determined, Eq. (2) is easily solved for $\tilde{E}_0$.

*To avoid complexities unrelated to lateral ionospheric gradients, our calculations ignore the earth's curvature--an approximation well justified for ELF propagation parameters other than spreading loss.

To characterize S_0 in physical terms, we note that at large lateral distances D from the source,

$$E_0 \propto \exp\ (-ikS_0D) \ . \tag{3}$$

Thus, ReS_0 is the ratio of the speed of light to the phase velocity of the waveguide mode, and ImS_0 is proportional to the attenuation coefficient α, such that

$$\alpha = -8.6kImS_0 \quad dB/Mm \ , \tag{4}$$

where k is in Mm^{-1}.

In the presence of lateral ionospheric gradients, a rigorous separation of variables is impossible. Hence, fields cannot be expressed as products of vertical and radial functions, as they are in Eq. (2). But when ionospheric irregularities are large enough to significantly affect ELF propagation, scales for lateral variations of the ionospheric refractive index tend to be at least ten times longer than those for vertical variations. It can therefore be argued that the waveguide propagation parameters depend mainly on the local ionosphere, and that separation of the fields into vertical and lateral functions is an approximately correct procedure.

Using the above argument, Field and Joiner [1979] combined eikonal and full-wave methods to calculate the fields in a laterally nonuniform waveguide. Their main approximation was to separate the ground-level fields into vertical and lateral functions, each of which was then computed on a full-wave basis. The ground-level field [note that $F(z = 0) = 1$] was assumed to be

$$E \approx A\Lambda(x, y)\tilde{E}(x, y) \ , \tag{5}$$

where the lateral dependence resides mainly in $\tilde{E}$, satisfying

$$\left[\nabla_T^2 + k^2S^2(x, y)\right] \tilde{E} = 0 \ . \tag{6}$$

The full-wave methods for obtaining S_0 and Λ_0 (given in the references cited above) can also be used to obtain $\Lambda(x, y)$ in Eq. (5) and $S(x, y)$ in Eq. (6). Such calculations must be carried out for many locations (x, y), each governed by a local ionospheric height profile, to well represent the lateral dependence of S and Λ. A single calculation of S_0 and Λ_0, on the other hand, suffices to represent all locations under laterally uniform conditions.

To calculate reflections from widespread disturbances that can be approximated as semiinfinite regions with diffuse boundaries, we solve Eq. (6) directly (see Sec. IV). To calculate the propagation anomaly due to a laterally bounded disturbance, however, it is convenient to recast the problem as an integral equation. A laterally nonuniform ionospheric disturbance can be characterized by the difference $S^2(x, y) - S_0^2$. The undisturbed wave function $\tilde{E}_0$ is governed by S_0 and can be assumed known. Subtracting Eq. (2) from Eq. (4) gives

$$(\nabla_T^2 + k^2 S_0^2)(\tilde{E} - \tilde{E}_0) = -k^2(S^2 - S_0^2)\tilde{E} \ . \tag{7}$$

Then, using the Green's function

$$G = -i\pi H_0^{(2)}(kS_0 r_2) \ , \tag{8}$$

where H is the Hankel function, and applying the two-dimensional Green's theorem, the integral equation for $\tilde{E}$ is obtained:

$$\tilde{E}(x, y) = \tilde{E}_0(x, y)$$

$$- \frac{ik^2}{4} \iint_{-\infty}^{\infty} dx' \, dy' \left[S^2(x', y') - S_0^2\right]$$

$$\cdot H_0^{(2)}(kS_0 r_2)\tilde{E}(x', y') \ . \tag{9}$$

Equation (9) is formally identical to an integral equation of Wait [1964]. The diagram of the propagation in Fig. 1 defines the geometric terms in the equations above.

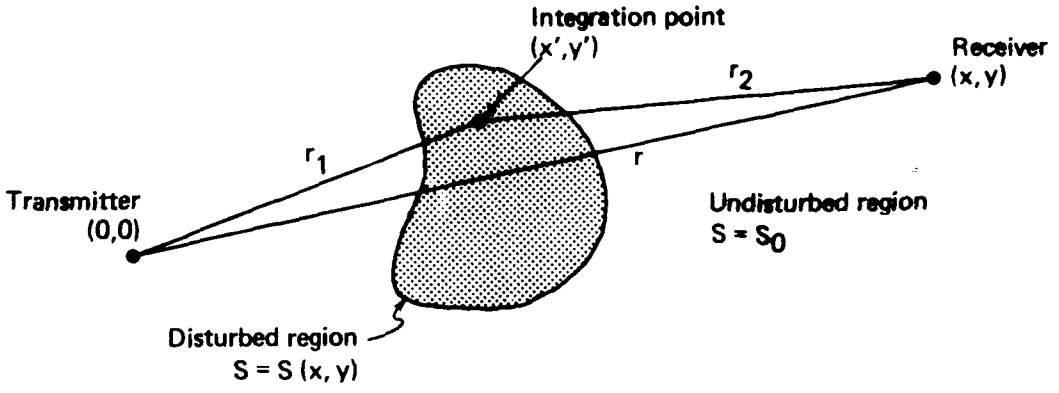

Fig. 1--Schematic of propagation for laterally bounded ionospheric disturbance

It is also convenient to define a relative propagation function W, denoting the fractional amount by which the disturbed lateral wave function $\tilde{E}$ differs from the undisturbed function $\tilde{E}_0$: specifically,

$$\tilde{E}(x, y) = W(x, y)\tilde{E}_0(x, y) \ . \tag{10}$$

Inserting Eq. (10) into Eq. (9) and expressing $\tilde{E}_0$ as for a horizontal electric dipole transmitter [Field and Joiner, 1979] gives

$$W(x, y) = 1 - \frac{ik^2}{4} \int\int_{-\infty}^{\infty} dx' \, dy' \left[S^2(x', y') - S_0^2 \right]$$

$$\cdot \left[\frac{x'r}{xr_1} \right] \frac{H_0^{(2)}(kS_0r_2) H_1^{(2)}(kS_0r_1)}{H_1^{(2)}(kS_0r)} \, W(x', y') \ , \tag{11}$$

which is the most general form of the integral equation for the relative propagation function.

III. MODELS OF WAVEGUIDE DISTURBANCES

The analytic models given below pertain to two types of waveguide disturbances--laterally bounded and widespread, both of arbitrary strength--that were not analyzed by Field and Joiner [1979]. The numerical results reported in Sec. V were obtained with the present models.

LATERALLY BOUNDED DISTURBANCE

A laterally bounded disturbance was schematically illustrated in Fig. 1. We represent the disturbed region by

$$S^2(x, y) - S_0^2 = \left[S_1^2 - S_0^2\right] \exp\left[-\frac{(x - \bar{x})^2}{(\Delta x)^2}\right] \exp\left[-\frac{(y)^2}{(\Delta y)^2}\right], \quad (12)$$

where S_1^2 denotes the value of the waveguide propagation constant at $x = \bar{x}$, $y = 0$. Note that Eq. (12) implies no limits on the strength $S_1 - S_0$; and that the disturbance is assumed to center on the x-axis, with off-path effects accounted for by adjusting the transverse location y of the receiver. Adjusting $S_1^2 - S_0^2$, $(\Delta x)^2$, $(\Delta y)^2$, and $\bar{x}$ hence allows the equation to represent disturbances with different strengths, lateral gradients, and longitudinal positions. The disturbance effectively vanishes when $|x - \bar{x}|$ or y becomes several times greater than Δx or Δy.

WIDESPREAD DISTURBANCE

The general features of the model for reflection from a widespread disturbance are illustrated in Fig. 2, showing (from the top) a plane waveguide mode with vertical electric field E_I incident at angle θ on a disturbed region, which is assumed stratified in one lateral dimension. Taking the direction of stratification to be parallel to the x-axis yields no loss of generality, so the disturbance has lateral variation only in the y-direction. (Recall that vertical variations

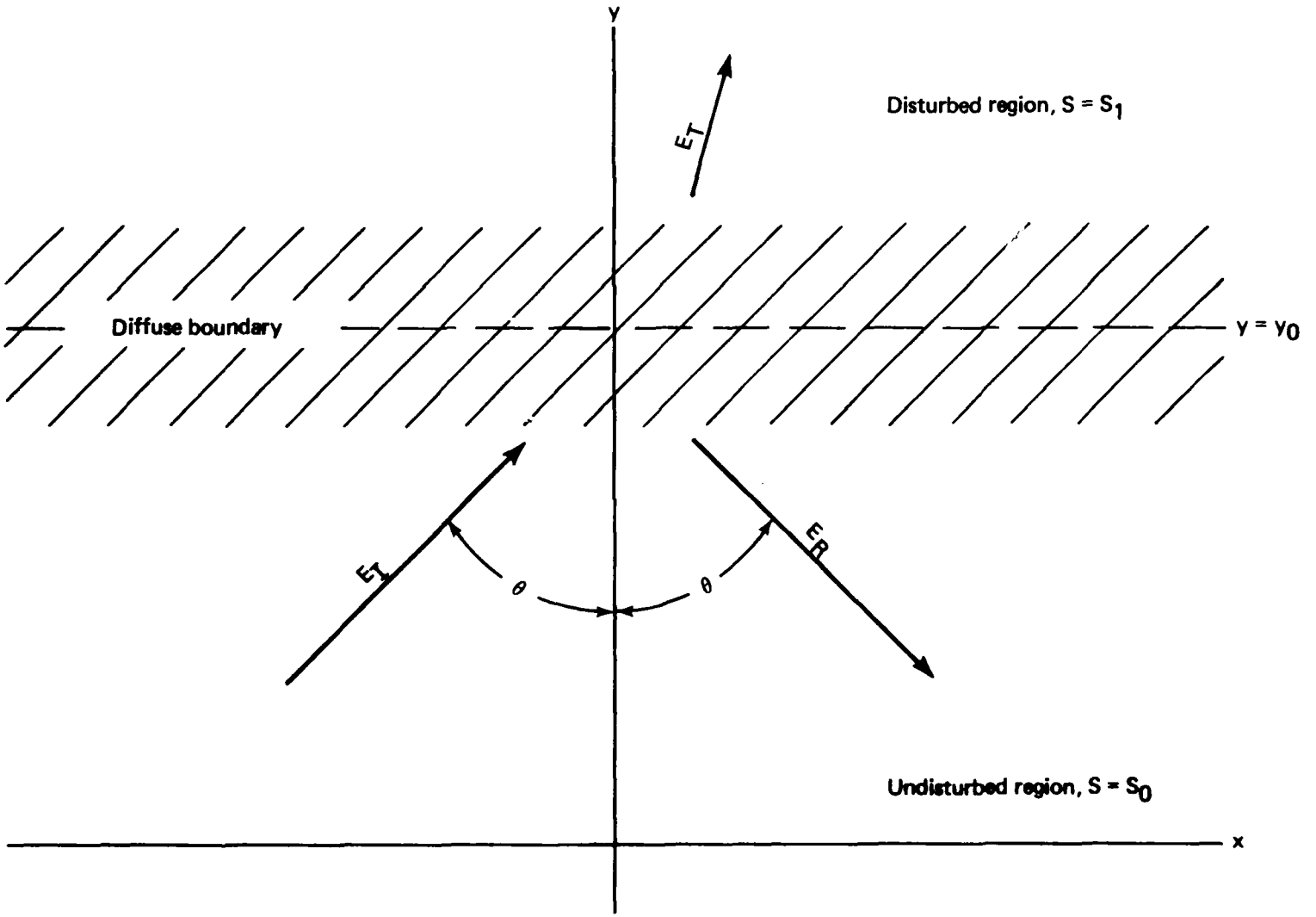

Fig. 2--Schematic of reflection from disturbed region with diffuse, stratified boundary. Arrows show direction of propagation; electric vectors point in z-direction.

in the ionosphere are accounted for in the waveguide propagation parameter S.) Our task is to compute the reflected signal E_R, which is ignored in the often-used two-dimensional WKB treatment of ELF propagation.

The uniform waveguide propagation constants S_0 and S_1 respectively characterize the undisturbed and disturbed regions. Lateral gradients in the boundary cause the partial reflection of the incident signal from the disturbed region. Under realistic conditions, disturbed regions of the ionosphere are separated from undisturbed regions by boundary regions whose widths compare with a reduced ELF wavelength $\lambda/2\pi$. Given those conditions, we cannot use either of the two usual approximations--abrupt boundary or slowly-varying boundary--to calculate the reflection coefficient. Instead, we must devise a model that fully accounts for the finite--but nonzero--gradients in the diffuse boundary, and permits an analytic solution to Eq. (6). The formula

$$S^2(y) = S_0^2 + \frac{(S_1^2 - S_0^2) \exp [(y - y_0)/\Delta y]}{1 + \exp [(y - y_0)/\Delta y]} \tag{13}$$

has the desired features: namely, $S(y) \to S_0$ in the undisturbed region; $S(y) \to S_1$ in the disturbed region; and the transition from S_0 to S_1 occurring continuously over a distance Δy, which can be varied to describe moderate, abrupt, or gradual boundaries centered at $y = y_0$.

Before deriving the lateral reflection coefficient, we consider the types of disturbances the model outlined by Fig. 2 and Eq. (13) can represent. The assumption of a stratified boundary applies only if the boundary curvature greatly exceeds $\lambda/2\pi$. Similarly, the assumption that the disturbance is of semiinfinite extent in the y-direction ignores reflections from the rear edge, although they must in principle exist on a sphere (the earth). Given that ELF waves are thousands of kilometers long and that $\lambda/2\pi$ is typically between 0.5 and 1 Mm, our model thus applies only to disturbances that cover large portions of the earth or to the diurnal effect on the waveguide, where the diffuse boundary represents the terminator.

IV. REFLECTION COEFFICIENT

This section derives an equation for the reflection coefficient, solving Eq. (6) for the waveguide model in Sec. III. Recall from Eq. (5) that $\tilde{E}$ [governed by Eq. (6)] must be multiplied by the local excitation factor Λ to obtain the true electric field. Both the incident and reflected waves have the same excitation factor, which therefore cancels, giving for the reflection coefficient

$$R = \frac{E_R}{E_I} = \frac{\tilde{E}_R}{\tilde{E}_I} = \tilde{R} \ . \tag{14}$$

However, the transmitted wave contains Λ_1 of the disturbed region of the waveguide, such that the true transmission coefficient is

$$T = \frac{E_T}{E_I} = \frac{\Lambda_1}{\Lambda_0} \frac{\tilde{E}_T}{\tilde{E}_I} = \frac{\Lambda_1}{\Lambda_0} \tilde{T} \ . \tag{15}$$

The difference between T and $\tilde{T}$ must be accounted for if transmission coefficients are to be calculated from the reflection coefficients given below. Unlike at higher frequencies, higher order modes generated by the boundary need not be considered at ELF, where all but the TEM mode are far below the cutoff frequency.

Substituting Eq. (13) into Eq. (6), and considering that $E \propto \exp(-ikx \sin\theta)$ for stratified media, we obtain the following form for the two-dimensional wave equation:

$$\frac{d^2}{dy^2} \tilde{E} + k_0^2 \left\{ \cos^2\theta + \frac{(N^2 - 1) \exp[(y - y_0)/\Delta y]}{1 + \exp[(y - y_0)/\Delta y]} \right\} \tilde{E} = 0 \ . \tag{16}$$

For Eq. (16) we define $N^2 = S_1^2/S_0^2$--physically signifying a complex refractive index--and $k_0^2 = k^2 S_0^2$--denoting the complex wave number in the undisturbed portion of the waveguide.

To calculate the reflection coefficient, we apply the following changes of variable to convert Eq. (10) to a standard form:

$$\tilde{E} = e^{-ik_0 \Delta y \cos\theta \zeta} (1 + e^{\zeta})\psi(\zeta) \ , \tag{17}$$

where $\zeta = (y - y_0)/\Delta y$. Considerable but straightforward rearrangement yields for ψ

$$(1 + e^{\zeta})\psi'' + [-2ik_0 \Delta y \cos\theta + (2 - 2ik_0 \Delta y \cos\theta)e^{\zeta}]\psi'$$

$$+ [1 - 2ik_0 \Delta y \cos\theta + k_0^2(\Delta y)^2(N^2 - 1)]e^{\zeta}\psi = 0 \ , \tag{18}$$

where a prime denotes differentiation with respect to ζ.

The form of Eq. (18) is such that hypergeometric functions can be used to derive the reflection coefficient. The procedure is only outlined here, since it is similar to that originally used by Epstein [1930]--and more recently documented by Budden [1961]--in studying the reflection and transmission of radio waves that are incident on the ionosphere from below. The derivation follows from recognizing that the solutions to the equation

$$(1 + e^{\zeta})\psi'' + [c - 1 + (a + b)e^{\zeta})\psi' + abe^{\zeta}\psi = 0 \tag{19}$$

are hypergeometric functions* of argument $\eta = -e^{\zeta}$ and η^{-1} that contain the usual coefficients; that is, the solutions to Eq. (19) are combinations of $F(a, b, c; \eta)$, $F(a, 1 - c + a; 1 - b + a; \eta^{-1})$, ..., where F is the standard hypergeometric function [Abramowitz and Stegun, 1964].

Well-known analytic continuation formulas connect the hypergeometric functions of argument η with those of argument η^{-1}. The

---

*By the change of variable $\eta = -e^{\zeta}$, Eq. (19) transforms to

$$\eta(1 - \eta)\frac{d^2\psi}{d\eta^2} + [c(a + b + 1)\eta]\frac{d\psi}{d\eta} - ab\psi = 0 \ ,$$

which is the best-known form of the hypergeometric equation.

leading terms of power-series expansions are then applied in both the undisturbed region, where $\eta << 1$, and the disturbed region, where $\eta^{-1} << 1$. The expansions contain readily identifiable terms such as E_I, E_R, and E_T, from which the reflection and transmission coefficients are easily formed. The steps are tedious but straightforward, and lead to the formula for the reflection coefficient [Budden, 1961]:

$$R = \frac{\Gamma(c - 1)\Gamma(1 - a)\Gamma(1 + b - c)}{\Gamma(c - a)\Gamma(b)\Gamma(1 - c)} , \tag{20}$$

where Γ is the gamma function [Abramowitz and Stegun, 1964].

The final step relates our model to the canonical result of Eq. (20) through the equivalence of Eqs. (18) and (19)--which obtains provided

$$\begin{aligned} a &= 1 - ik_0 \Delta y(\cos\theta + q_1) , \\ b &= 1 - ik_0 \Delta y(\cos\theta - q_1) , \\ c &= 1 - 2ik_0 \Delta y \cos\theta , \end{aligned} \tag{21}$$

where

$$q_1^2 = S_1^2/S_0^2 - \sin^2\theta . \tag{22}$$

Substituting Eq. (21) into Eq. (20), and using the identity $\Gamma(1 + z) = z\Gamma(z)$, we have

$$R = R_0(\theta)\, D(\theta, \Delta y) , \tag{23}$$

where

$$R_0(\theta) = \frac{\cos\theta - q_1}{\cos\theta + q_1} \tag{24}$$

is the Fresnel coefficient for reflection from a sharp boundary, and

$$D(\theta, \Delta y) = \frac{\Gamma(1 - 2ikS_0\,\Delta y\cos\theta)\Gamma^2[1 + ikS_0\,\Delta y(q_1 + \cos\theta)]}{\Gamma(1 + 2ikS_0\,\Delta y\cos\theta)\Gamma^2[1 + ikS_0\,\Delta y(q_1 - \cos\theta)]} \tag{25}$$

is a diffuseness factor that accounts for the reduced reflection due to the nonabruptness of the boundary. It is easily shown that $|D|$ becomes smaller as Δy increases. Moreover, when $\Delta y = 0$, $D = 1$, and Eq. (23) reduces to the Fresnel coefficient R_0.

V. NUMERICAL RESULTS

This section presents numerical results for the modal reflection from a disturbed region of semiinfinite extent and for the relative propagation functions for laterally bounded disturbed regions. To emphasize reflection phenomena, most reflection coefficients are calculated for 45 Hz, the lowest ELF transmitting frequency. The relative propagation function is calculated for 75 Hz.

SEMIINFINITE DISTURBED REGION

In the following pages, the reflection coefficient R [calculated from Eq. (23)] is plotted as a function of incidence angle θ and boundary-thickness-parameter Δy. In all but one case the incident and reflected waves are assumed to be in the ambient daytime region of the earth, where the waveguide propagation constant is S_0 (see Fig. 2). We assume $S_0 = 1.2 - 0.09i$ at 45 Hz and $S_0 = 1.15 - 0.085i$ at 75 Hz, corresponding to daytime attenuation rates of 0.73 dB/Mm and 1.15 dB/Mm. Those figures agree reasonably well with both measured and calculated values [e.g., Pappert and Moler, 1974; Ginsberg, 1974; Galejs, 1972], although S_0 depends somewhat on propagation direction, latitude, and season, and values larger or smaller than those here have been reported.

The table below gives the values of S_1 used to calculate the reflection coefficient. The various SPE entries are averages based on numerous calculations performed over several years [e.g., Field, 1969]. (The strong SPE model also applies to a moderate nuclear disturbance.) The value for the nighttime propagation constant is rather problematic, in that experimental measurements exhibit much scatter [Bannister, 1974; White and Willim, 1974]. Moreover, the measured nighttime attenuation rates tend to be somewhat larger than those calculated from the accepted model ionospheric height profiles [Pappert and Moler, 1974]. Nevertheless, both measurements and calculations show that the attenuation rate and ReS are usually smaller at night than in the daytime. The ambient night value shown for S_1 in the table is therefore slightly smaller than the ambient day value for S_0 given above.

VALUES OF S_1

Condition	Frequency (Hz)	Attenuation Rate, α (dB/Mm)	S_1
Strong SPE	45	2.4	1.75-0.3i
	75	3.4	1.50-0.25i
Moderate SPE	45	1.6	1.45-0.2i
Weak SPE	45	1.3	1.35-1.16i
Ambient night	45	0.6	1.15-0.075i

Figures 3 through 6 plot R against the incidence angle of an ELF waveguide mode impinging on the boundary that separates the ambient daytime region of the earth from each SPE in the table. In Fig. 7, R is plotted for a mode incident on the day/night terminator from the nighttime side, and in Fig. 8, for a mode incident from the daytime side. In all these figures, the curve R_0 is the Fresnel reflection coefficient, which applies if the two regions are separated by a sharp boundary [see Eq. (23)]. The remaining curves, which account for the diffuseness of the boundary, result from multiplying R_0 by the diffuseness factor [Eq. (25)]. Their labels quantify the effective boundary thickness Δy.

The reflection coefficient has several common features in Figs. 3 through 6 that are relatively insensitive to SPE strength. First, it is small--less than a few tenths--for all but the most oblique incidence angles. Second, it is much reduced by the diffuseness of the boundary, particularly if the boundary-transition width Δy is greater than $\lambda/2\pi$. Third, it is smaller at 75 Hz than at 45 Hz, although its sensitivity to the transition width Δy is greater at the higher frequency (compare Fig. 3 with Fig. 4).

Satellite data [Reagan and Watt, 1976] show that the energetic proton flux during the August 1972 SPE was nearly constant at invariant latitudes above ~65 deg, rolling off rapidly outside the polar cap and diminishing an order of magnitude over 3 to 5 deg of latitude. Since

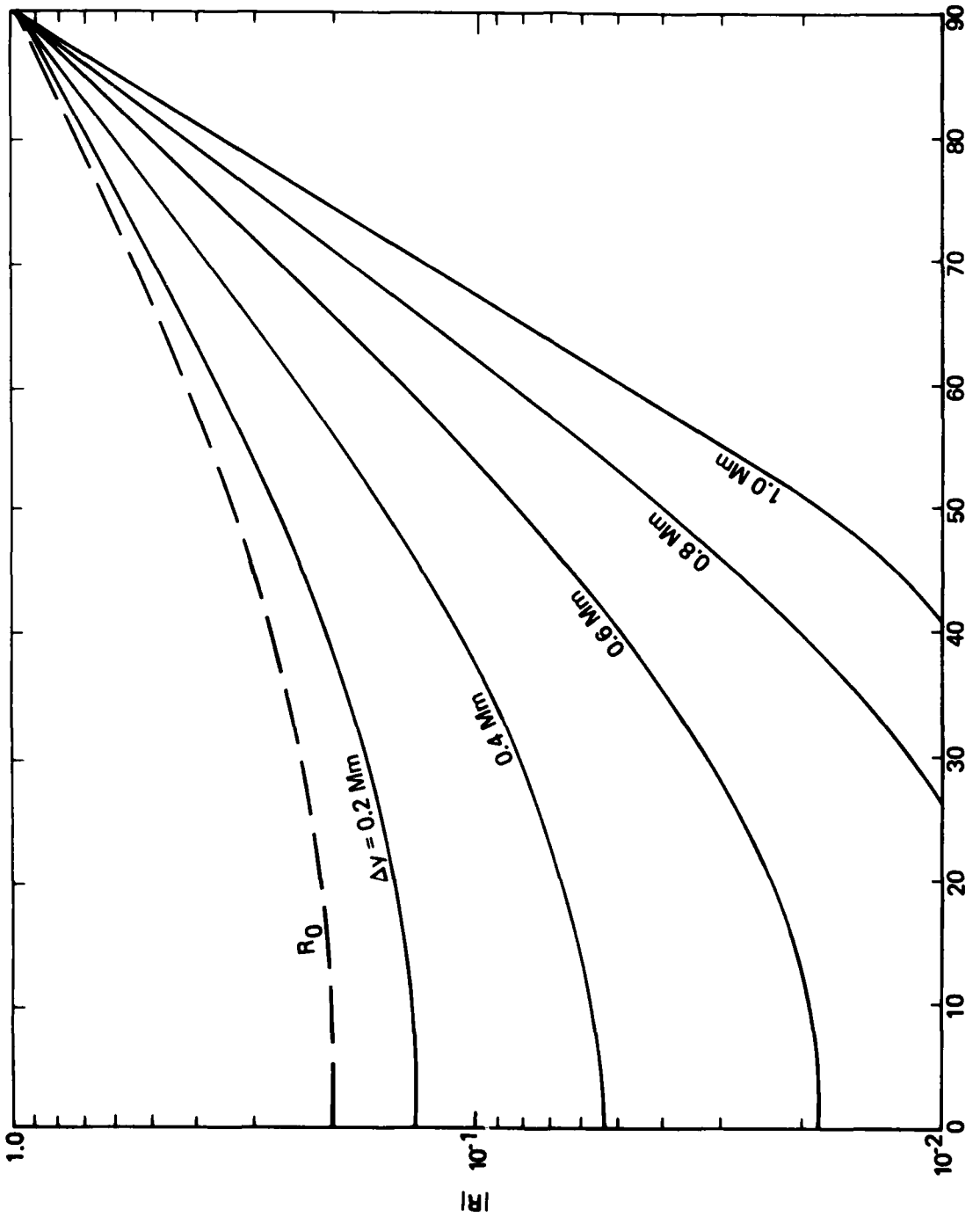

Fig. 3--Reflection from strong SPE (F = 45 Hz)

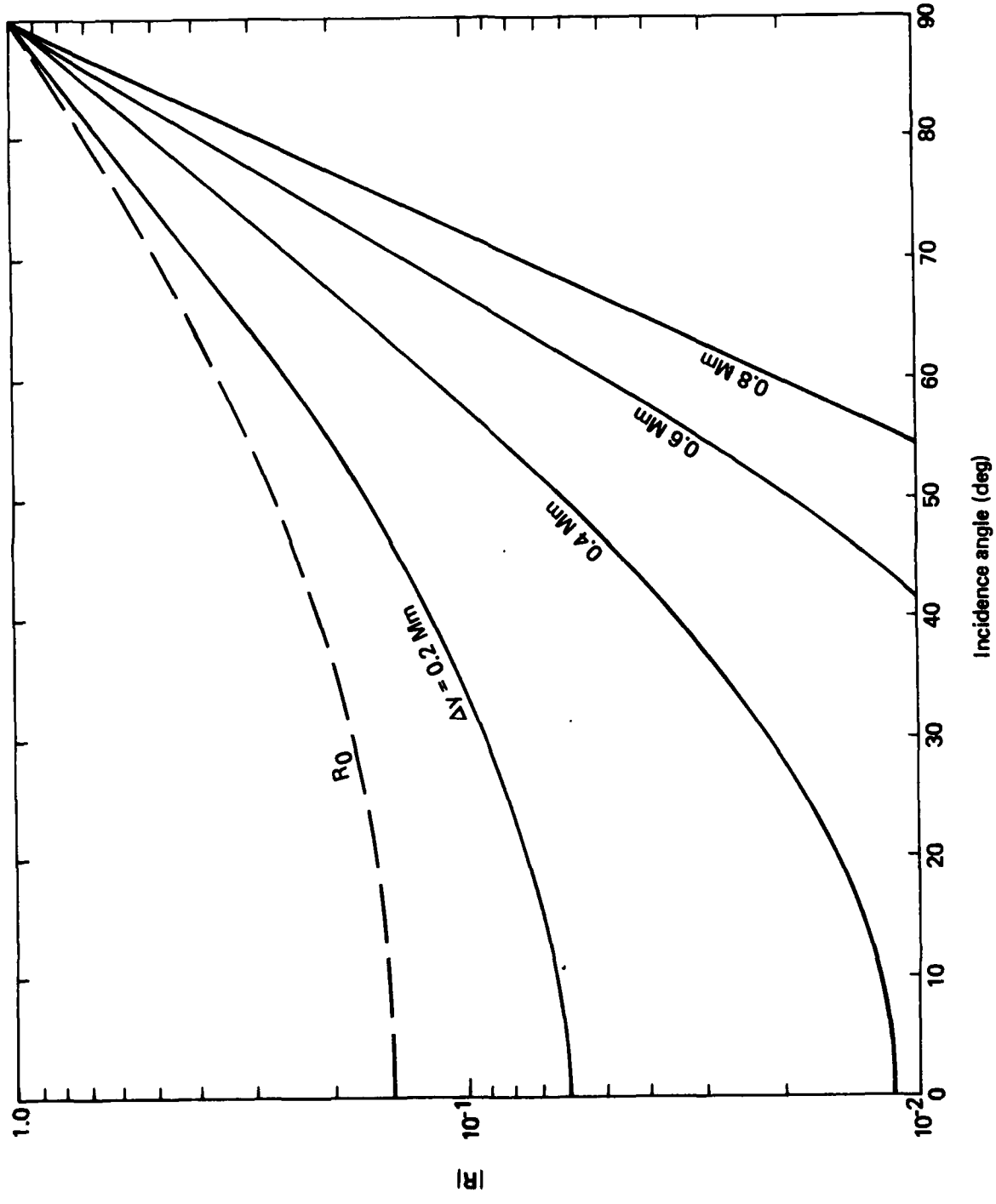

Fig. 4--Reflection from strong SPE (F = 75 Hz)

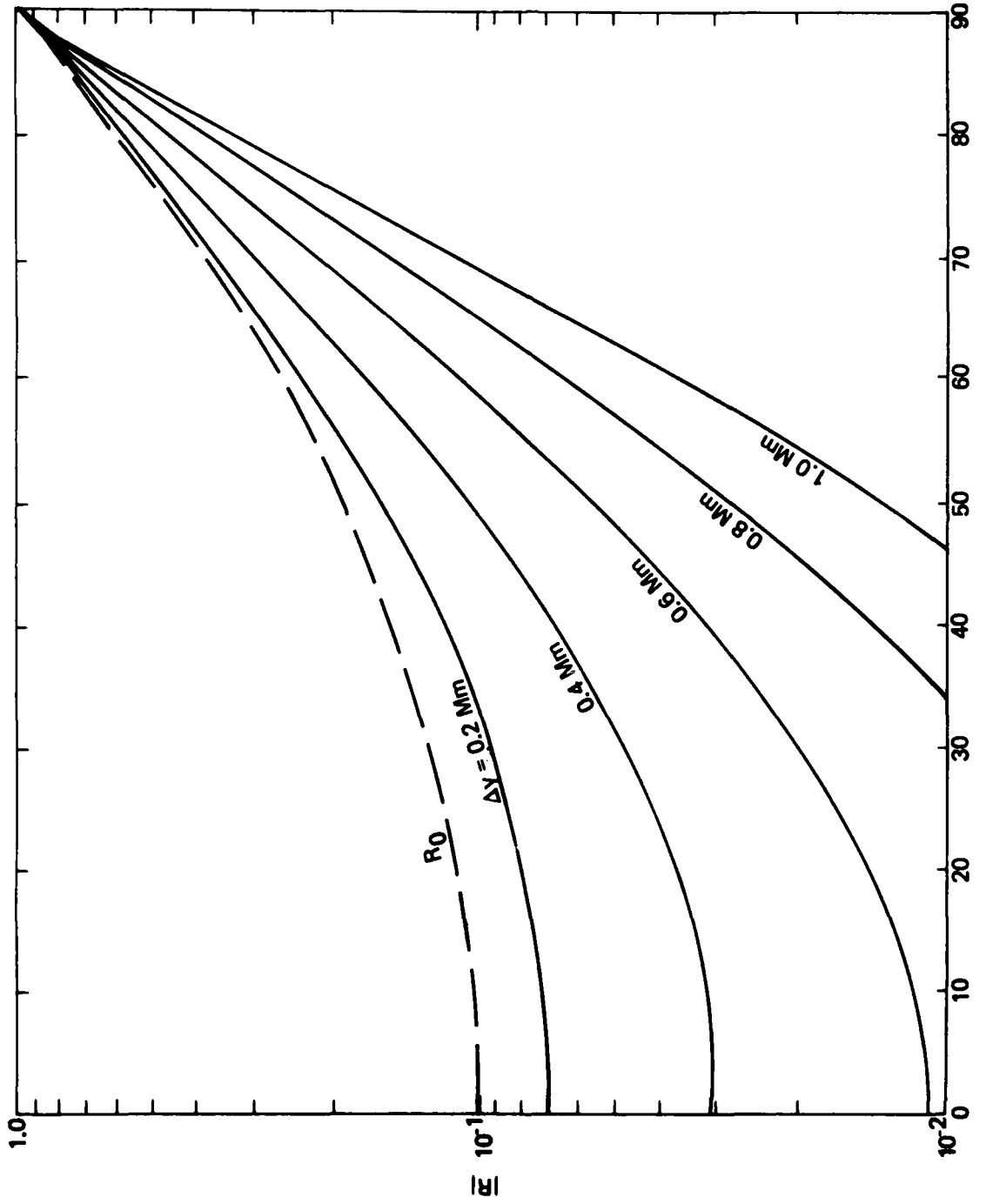

Fig. 5--Reflection from moderate SPE (F = 45 Hz)

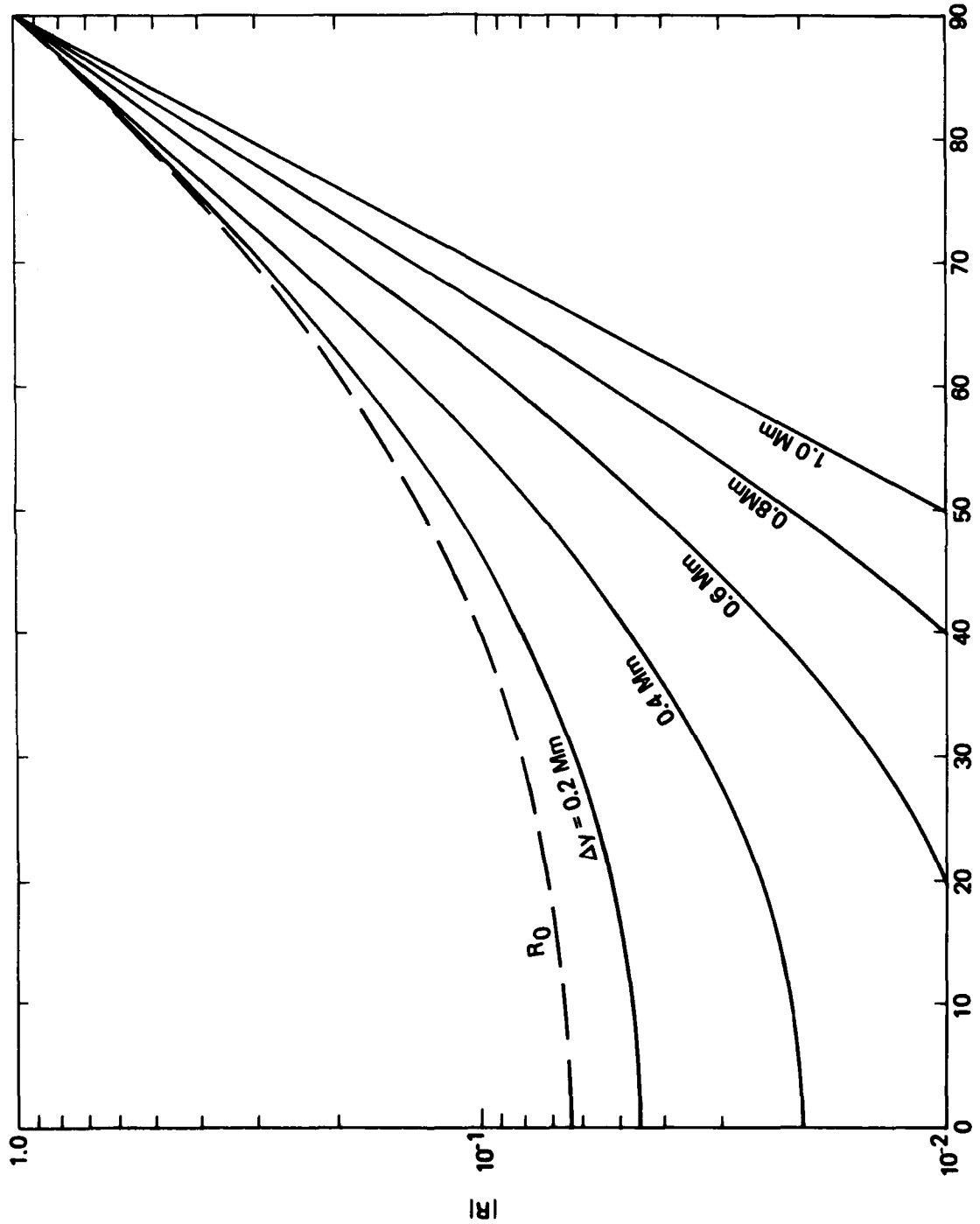

Fig. 6--Reflection from weak SPE (F = 45 Hz)

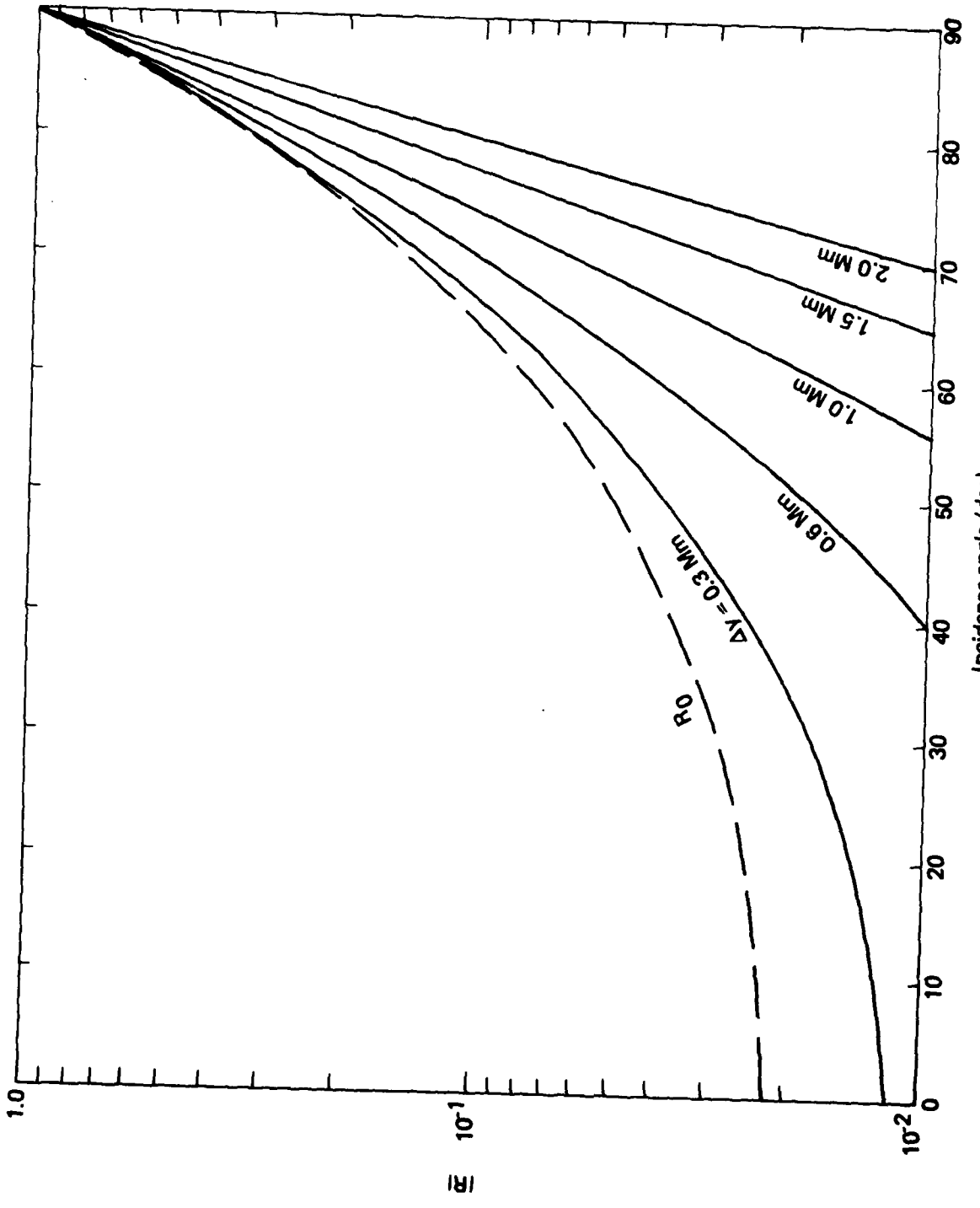

Fig. 7--Reflection from day/night terminator: mode incident from nighttime side (F = 45 Hz)

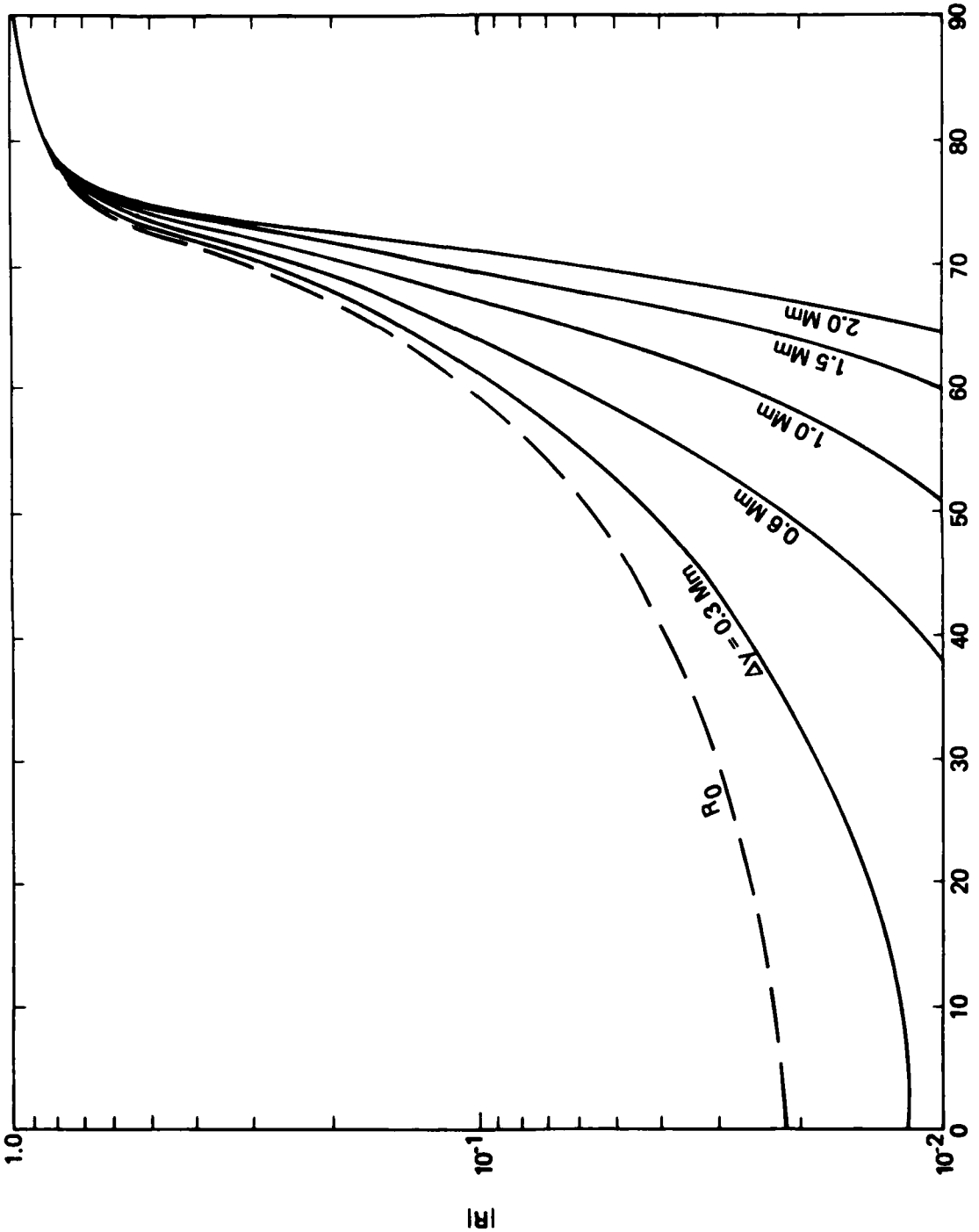

Fig. 8--Reflection from day/night terminator: mode incident from daytime side (F = 45 Hz)

1 deg of latitude corresponds to approximately 100 km of lateral distance, we infer that $\Delta y \approx 300$ to 500 km reasonably represents an actual SPE. For that Δy, significant reflection ($|R| \gtrsim 0.7$) will occur if the TEM mode is incident on the SPE boundary at angles greater than 80 to 85 deg (see Figs. 3 through 6).

Such oblique incidence angles may actually occur on continental U.S.-North Atlantic ELF paths that are nearly tangent to the polar cap. Just outside the cap, we would expect interference patterns between the direct ELF mode and that obliquely reflected by an SPE. In addition, since poor transmission occurs for incidence angles at which the reflection coefficient is large, receivers on paths that obliquely intersect the polar cap will be in "shadow zones" during an SPE, with signals degraded by reflection beyond the amount due to the increased α associated with the SPE (see the table presented earlier).

Our discussion considers only the reflection of modes incident on the SPE from an undisturbed region, it being unlikely that an ELF transmitter will ever be placed within the polar cap. But, since a transmitter must operate under both nighttime and daytime conditions, we consider both the reflection of waves incident from the night side of the terminator and those from the day side (see Figs. 7 and 8). From data on diurnal phase shifts for north-south VLF paths [Chilton, Crombie, and Jean, 1961], the earth-ionosphere waveguide makes the transition from daytime to nighttime propagation conditions in 60 to 90 min, during which time the earth's surface rotates some 1500 to 2500 km. Hence, the thickness of the day/night terminator is greater than the several-hundred-kilometer thickness of the SPE boundary. The values of Δy used to construct Figs. 7 and 8 are therefore greater than those used for Figs. 3 through 6.

Figure 7 shows that the reflection coefficient for night-to-day propagation is very small for all realistic incidence angles, and that the terminator would only slightly affect ELF signal strength. Such is as expected, because the difference $S_0 - S_1$ is small for night-to-day propagation and the boundary is very diffuse.

The results for day-to-night propagation (Fig. 8) are at first surprising. Although R is small (as expected) for small-to-intermediate

incidence angles, it becomes large ($|R| > 0.7$) for oblique incidence--a phenomenon analogous to the total internal reflection that occurs when a light wave propagates from glass to air. For the assumed day-to-night propagation parameters, $S_1 < S_0$ (see p. 15), and the reflection coefficient becomes large when the critical incidence angle

$$\theta_c \approx \text{Arc sin } S_1/S_0 \approx 75 \quad \text{deg}$$

is exceeded. In fact, only the complex nature of S_0 and S_1 prevents the reflection from being total for $\theta > \theta_c$.

The internal reflection shown in Fig. 8 will usually be unimportant because ELF paths tend to be east-west rather than north-south. However, it could prevent a daytime transmitter in the northern hemisphere from reaching a nighttime receiver in the southern hemisphere if the incidence angle on the terminator exceeded the critical angle, depending on the day and night waveguide parameters.

BOUNDED DISTURBANCE

The algorithm used to solve Eq. (11) is the subject of the Appendix. The numerical results given below illustrate the dependence of the fields on the strength, location, and extent of the disturbance. Although the results pertain to the analytic model defined in Eq. (12), the algorithm will work equally well for any spatial dependence $S(x, y)$, provided only that $S(x, y) - S_0$ effectively vanishes outside a rectangle several megameters on a side.

All results pertain to a frequency of 75 Hz, and as above, $S_0 = 1.15 - 0.085i$ characterizes the undisturbed portion of the waveguide. The propagation constant S_1 at the center of the disturbance is taken to be

$$S_1 = A(1.5 - 0.25i - S_0) + S_0 \ ,$$

so that strong, moderate, and weak disturbances can be modeled by letting $A = 1$, $2/3$, or $1/3$. For $A = 1$, S_1 assumes the value given earlier for a strong SPE.

Figure 9 plots W versus the off-path distance y for a strong (A = 1), longitudinally confined (Δx = 0.5 Mm) disturbance, with curves shown for several effective half-widths Δy.* In Fig. 9a, W is computed from the simple nondeviative WKB formula

$$W_{WKB} \sim \exp\left\{-ik \int_0^r [S(x', y') - S_0]\, dr'\right\} , \qquad (26)$$

where the integration path is the straight line connecting transmitter and receiver. Equation (26) is shown in the figure to give the intuitively expected result; namely, W is smallest for y = 0, where the direct path intersects the peak of the disturbance, and approaches unity for y >> Δy--in which case the direct path effectively misses the disturbance.

On the other hand, W calculated from the integral equation [Eq. (11)] is shown in Fig. 9b to exhibit a characteristic pattern on the line x = 10 Mm: a maximum for y = 0, a minimum a few megameters off-path, and increasing with off-path distance. That counterintuitive--but correct--full-wave behavior of W is due to focusing and diffraction--the effects of which are ignored in the nondeviative WKB formula.

Focusing occurs because wave normals tend to bend toward regions where S(x, y)--which in the waveguide formulation is analogous to the refractive index--is large. The disturbance therefore behaves as a converging cylindrical lens. Diffraction occurs because the effective aperture filled by the lens is approximately $2\Delta y$, which is smaller than or comparable to a Fresnel zone for the parameters used

*To minimize computation time, the results in this subsection are calculated for a longitudinal half-width Δx = 0.5 Mm. The effect of the disturbance is therefore modest, and W is within 20 to 30 percent of unity for all cases. A larger value for Δx would increase the anomalous attenuation and therefore yield a W much less than unity. Except as noted, the choice of Δx affects the results only in detail; it does not alter the overall conclusions. In Fig. 9 and subsequently, the total pathlength for y = 0 is 10 Mm, and the disturbance is centered at midpath ($\bar{x}$ = 5 Mm).

(a) WKB approximation

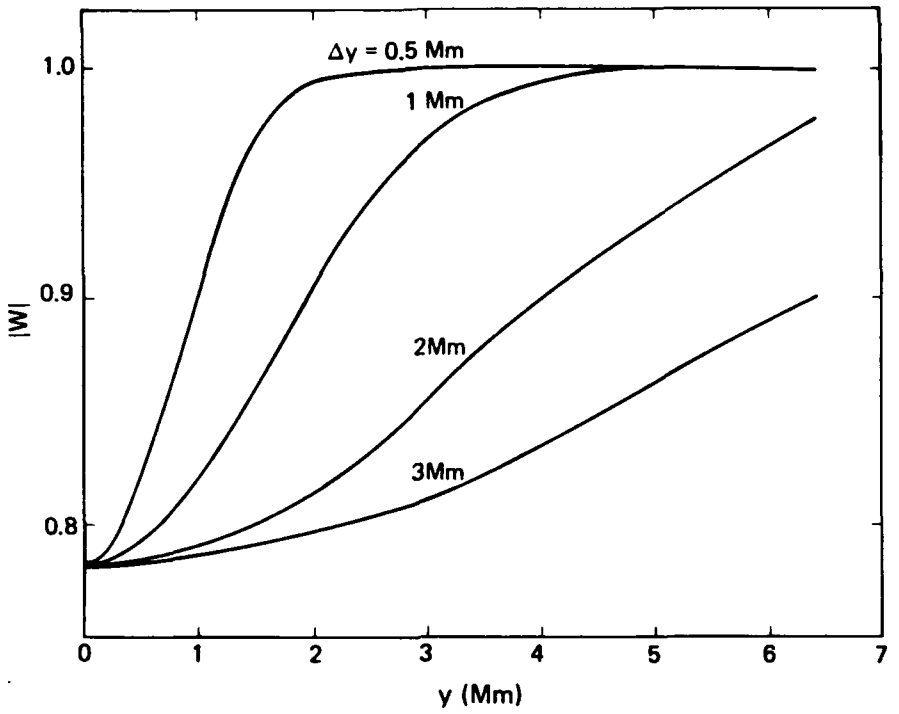

(b) Integral equation

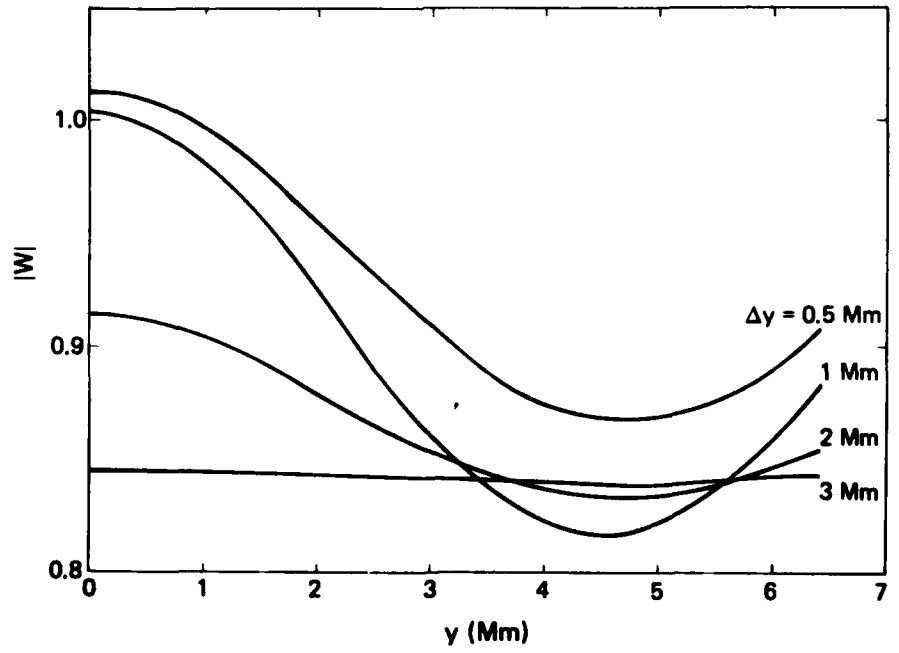

Fig. 9--Amplitude of W versus off-path distance y for x = 10 Mm, $\bar{x}$ = 5 Mm, Δx = 0.5 Mm, and strong (A = 1) disturbance with various half-widths

here. As expected, the diffraction/focusing pattern becomes much less pronounced as $2\Delta y$ approaches the width of the first Fresnel zone. Focusing may actually overcome the anomalous attenuation through the center of the disturbance, causing $|W|$ to exceed unity (see Fig. 9b).

Figure 10 is analogous to Fig. 9, except that the curves are parametric in disturbance strength rather than in transverse half-widths. As expected, the effects of lateral focusing are most pronounced for the strongest disturbance. A direct path that intersects the peak of the disturbance (receiver at $y = 0$) is illustrated in Fig. 11, showing the dependence of W on the transverse half-width Δy and treating disturbance strength parametrically. For reasons discussed above, signal strength W tends to decrease as the disturbance broadens (Δy increases) and strengthens (A increases).

To assess the relationship between W and the transverse dimension Δy of a disturbance, it is useful to define a transverse shape factor Q, such that

$$Q = \frac{W - 1}{W_{WKB} - 1} . \tag{27}$$

For a disturbance centered on the direct path, the WKB solution ignores transverse variations. Thus, Eq. (27) is the ratio of the correctly computed propagation anomaly to that computed by ignoring transverse gradients.* Since the WKB solution overestimates the anomaly by accounting for only the peak of an on-path disturbance, Q is everywhere smaller than unity.

For long paths and very weak disturbances satisfying the conditions

$$k|S_0|x >> 1 , \tag{28}$$

$$\frac{k^2|S_1^2 - S_0^2|(\Delta x)^2}{4} << 1 , \tag{29}$$

*Strictly speaking, the WKB solutions also ignore backward reflections. However, the effect on the received signal is small enough to be safely ignored here.

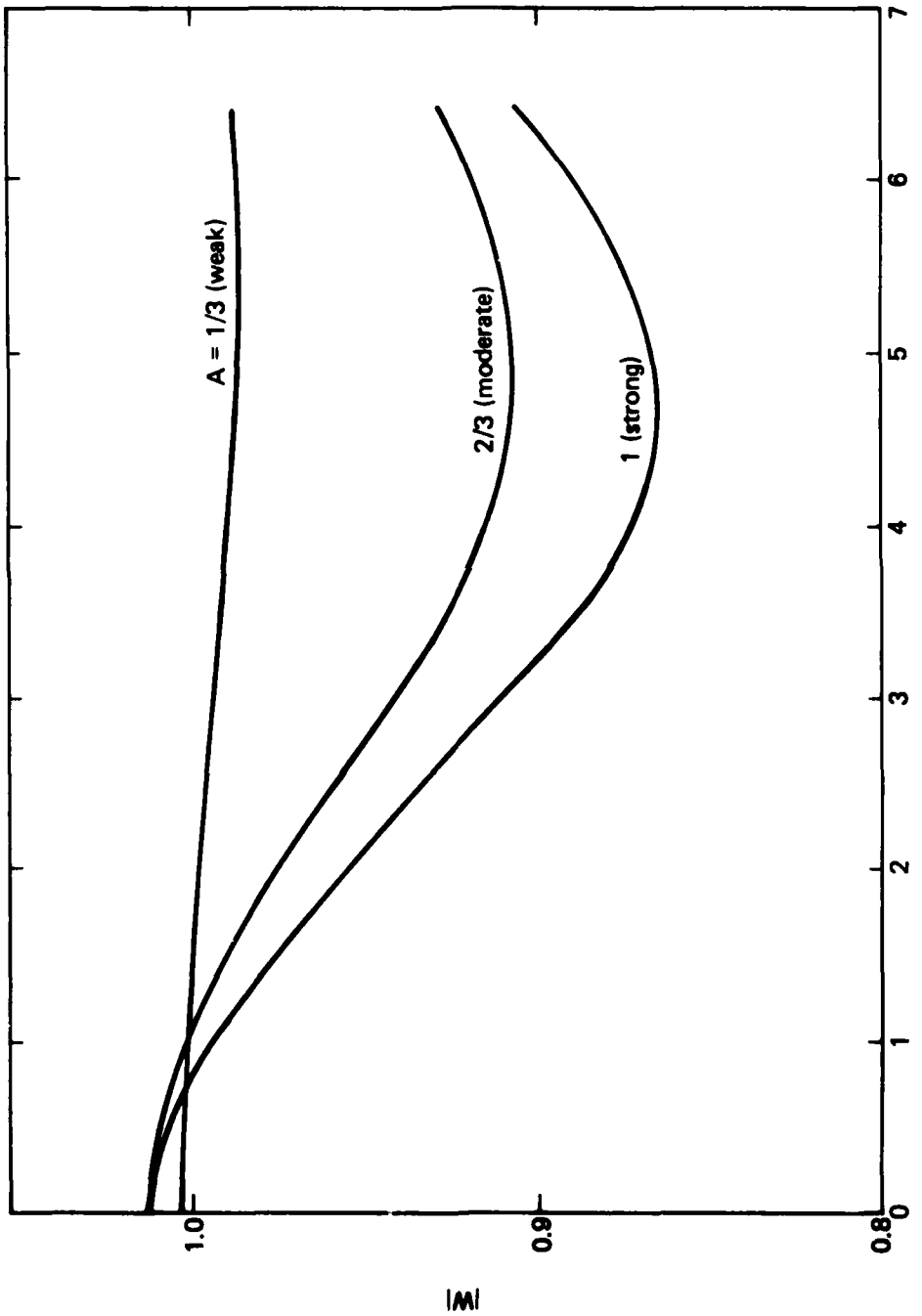

Fig. 10--Amplitude of W versus off-path distance y for x = 10 Mm, $\bar{x}$ = 5 Mm, $\Delta y = \Delta x = 0.5$ Mm, and various disturbance strengths

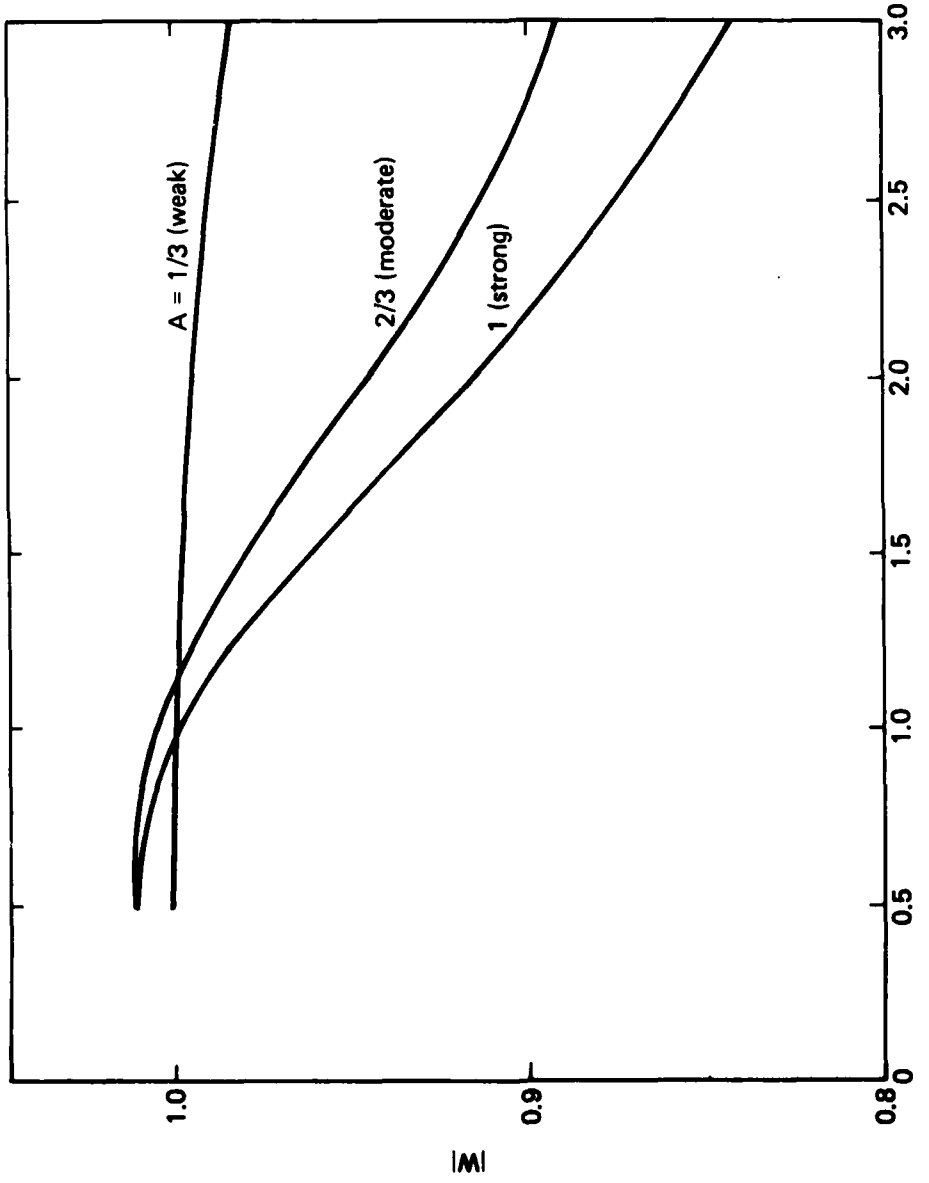

Fig. 11--On-path amplitude of W versus disturbance half-width Δy for $x = 10$ Mm, $\bar{x} = 5$ Mm, $\Delta x = 0.5$ Mm, $y = 0$, and various disturbance strengths

and

$$\frac{|S_1^2 - S_0^2|}{16S_0^2} \ll 1 \ . \tag{30}$$

Field and Joiner [1979]--using a perturbation method equivalent to the first Born approximation--showed that W has the limiting form

$$Q \xrightarrow[S_1 \to S_0]{} \Gamma^{1/2} = \left[1 - \frac{i}{\pi}\left(\frac{d}{\Delta y}\right)^2\right]^{-1/2} , \tag{31}$$

where d, the maximum half-width of the first Fresnel zone, is given by

$$d = \frac{1}{2}\left[\frac{x\lambda}{S_0}\right]^{1/2} . \tag{32}$$

Equation (31) shows that $Q \to 1$ and the transverse gradients can be safely ignored if $\Delta y > d$, so that the peak of the disturbance effectively fills the first Fresnel zone. Conversely,

$$|Q| \approx \frac{\sqrt{\pi}\ (\Delta y)}{d} \quad \text{if} \quad \frac{\Delta y}{d} \ll 1 , \tag{33}$$

giving the realistic result that for y = 0, the ratio of the actual attenuation to that calculated from the WKB formula (ignoring the finite transverse gradients) corresponds to the fraction of the first Fresnel zone filled by the disturbance.

Figure 12 shows Q computed numerically from Eq. (33) for three values of the strength parameter A. For comparison, the limiting value* given by Eq. (31) is also plotted. The simple limiting form for Q is remarkably accurate even for A = 1 (a very strong ionospheric disturbance).

To illustrate the longitudinal dependence of the field, Fig. 13 plots |W| versus x for a strong disturbance of longitudinal half-width

*$S_1 \to S_0$ implies $A \to 0$.

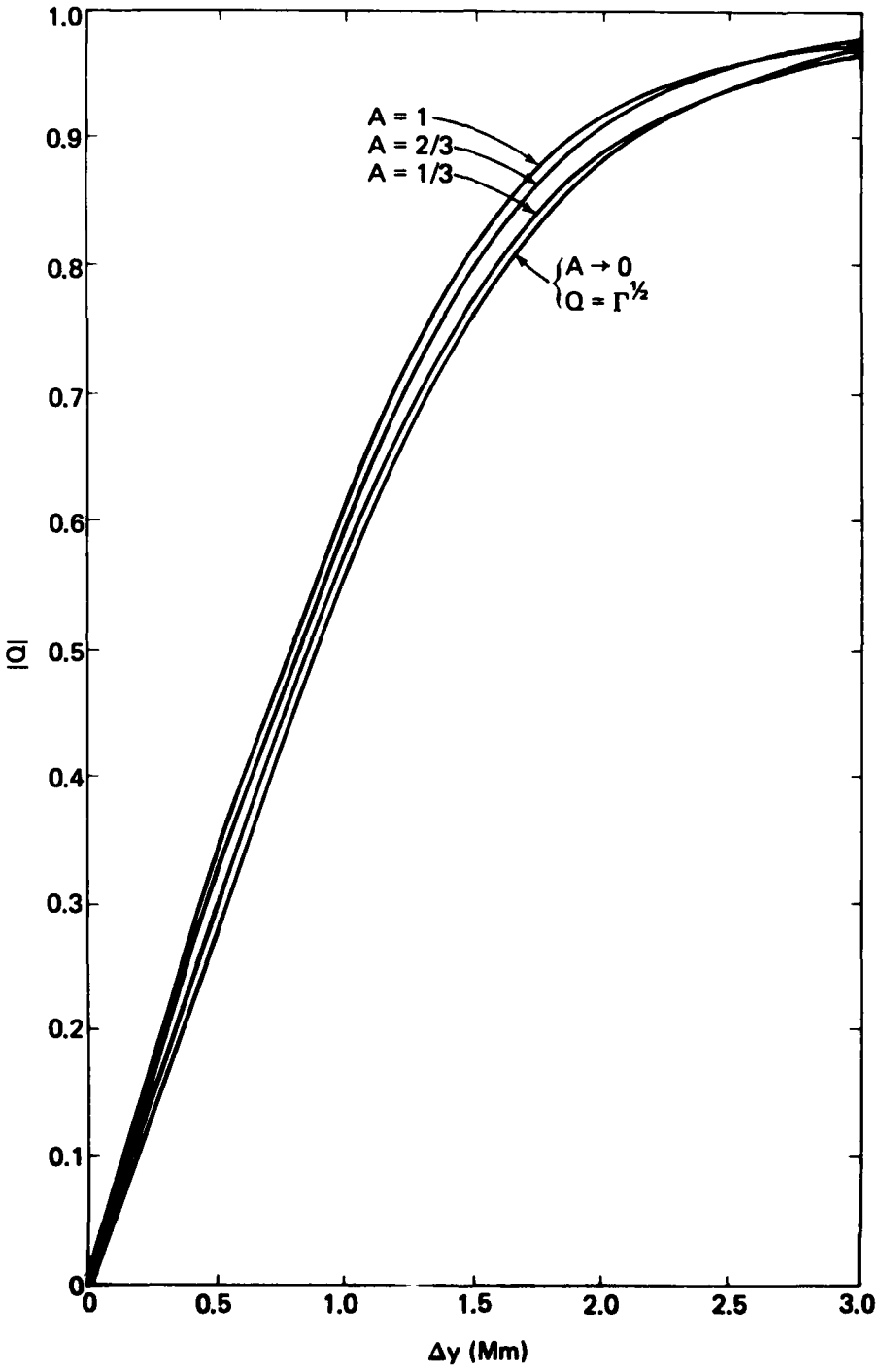

Fig. 12--Amplitude of transverse shape factor Q versus disturbance half-width Δy for disturbance centered on direct propagation path (y = 0)

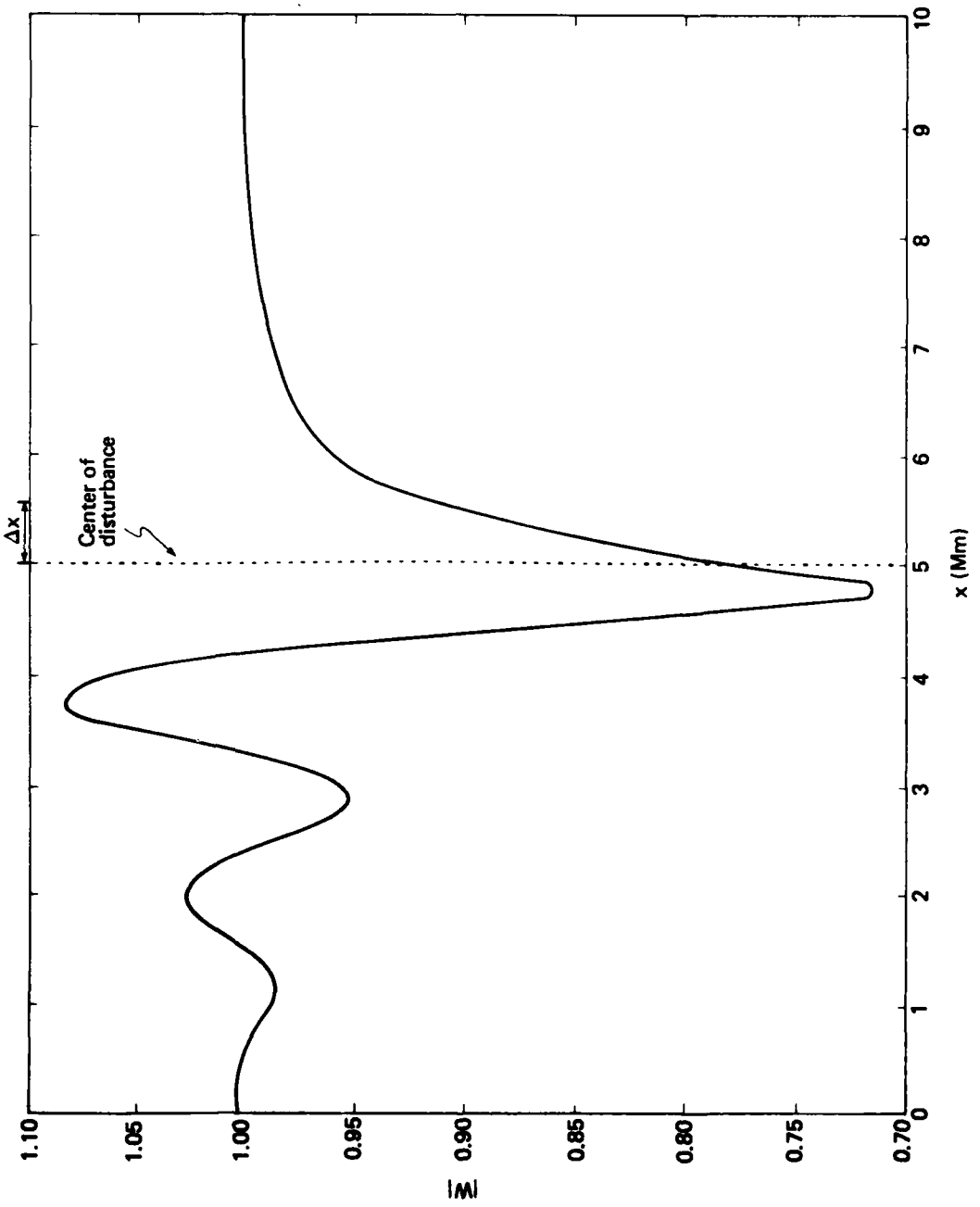

Fig. 13--Amplitude of W versus distance along direct propagation path for strong disturbance (A = 1, y = 0, Δy = 1 Mm)

Δx = 0.5 Mm and transverse half-width Δy = 1 Mm, centered on the direct path. The standing wave pattern in front of the disturbance is caused by reflections from the severe longitudinal gradients; it is much less pronounced for larger values of Δx. $|W|$ gradually increases with distance behind the disturbance, inasmuch as focusing causes energy to converge on the plane y = 0. For certain off-axis positions of the receiver, the electric field slowly decreases with distance.

APPENDIX

Numerically calculating the effect of a localized perturbation in the waveguide reduces to

1. Solving Eq. (11) [p. 6] in the disturbed region.
2. Integrating Eq. (11) over the disturbed region to obtain $W(x, y)$.

Assuming a localized perturbation, $S^2 - S_0^2$ vanishes outside some bounded region, allowing us to partition the region into a grid such that Eq. (11) takes the form

$$W(x, y) = 1 + \sum_{i=0}^{n-1} \iint_{S_i} dx'\, dy'\, K(x, y, x', y')W(x', y') \,, \qquad (A.1)$$

where S_i denotes n squares centered at x_i, y_i in the grid. Figure A.1 illustrates the partition for solution within a disturbance (shaded portion); Fig. A.2, the partition for outside a disturbance.

SOLUTION WITHIN DISTURBED REGION

Equation (A.1) may be rewritten

$$W(x_0, y_0) = 1 + \iint_{S_{(i=0)}} dx'\, dy'\, K(x_0, y_0, x', y')W(x', y') + \sum_{i=1}^{n-1} \iint_{S_i} dx'\, dy'\, K(x_0, y_0, x', y')W(x', y') \,, \qquad (A.2)$$

where $W(x_0, y_0)$ indicates that the solution point resides in square 0. Assigning every square the index 0 in sequence makes Eq. (A.2) rigorously equivalent to Eq. (A.1). It follows from Eq. (A.2) that

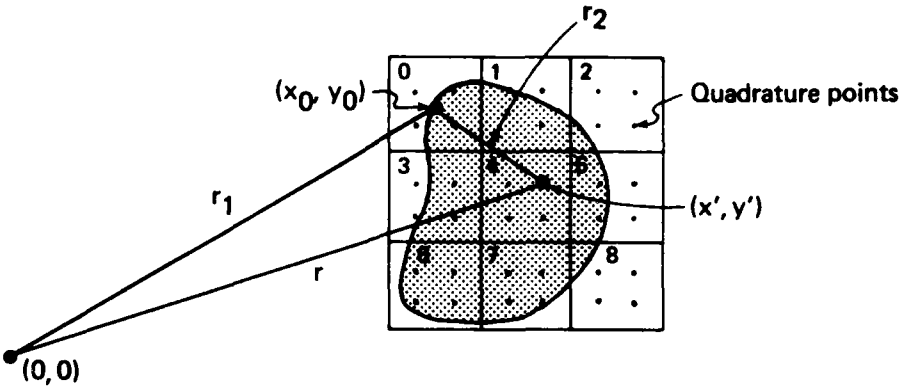

Fig. A.1--Partition for solution within disturbed region

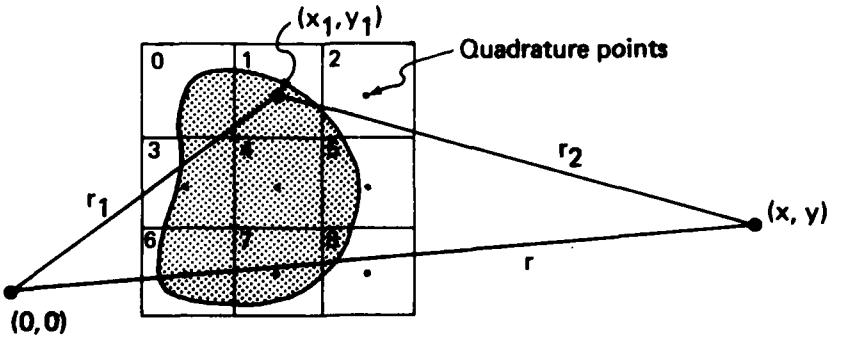

Fig. A.2--Partition for solution outside disturbance

$$W(x_0, y_0) \cong \frac{1 + \sum_{i=1}^{n-1} W(x_i, y_i) \iint_{S_i} dx'\, dy'\, K(x_0, y_0, x', y')}{1 - \iint_{S_0} dx'\, dy'\, K(x_0, y_0, x', y')} . \quad (A.3)$$

Equation (A.3) entails the approximation that for a sufficiently fine grid, $W(x', y') \approx W(x_i', y_i')$, the value at the center of any square, and may hence be factored out of that integral. The kernel K is integrated with standard quadrature methods over squares i = 1 to n - 1. Square 0 contains a subgrid to accommodate the singularity of K due to $H_0^{(2)}(kS_0r_2)$.

The algorithm becomes an iterative solution of Eq. (A.3), where all W are initially set to one. A single iteration consists of n solutions in which every square assumes an index in the permutation cycle 0, 1, 2, 3, ... n - 1. To evenly distribute error throughout the grid, the cycle starts at different places in different iterations.

Since only a few kernel functions need be evaluated, the algorithm is easily optimized by storing kernels rather than recomputing them; the kernel factors recur both from iteration to iteration (a self-evident recurrence) and within each iteration (not as self-evident but more important).

Arbitrary convergence criteria may be used. In the present problem, iterations stop at the same count regardless of whether we use a mean square or a maximum inter-iteration error measure. The size of the grid squares must be carefully chosen, since the computation time required for a solution varies as the fourth power of the number of squares.

SOLUTION OUTSIDE DISTURBANCE

The second part of the calculation is straightforward. With a receiver outside the disturbance, there is no problem of singularity of the kernel. Equation (A.1) may then be solved with simple quadrature techniques, where W inside the disturbed region is known from the

first part of the calculation. Only the geometric significance of terms in the kernel changes; distance from the observation point to the disturbance is now the most important factor, whereas in the solution within the disturbance, the squares adjacent to square 0 dominated.

REFERENCES

Abramowitz, M., and I. A. Stegun, *Handbook of Mathematical Functions*, U.S. Department of Commerce, National Bureau of Standards, Applied Mathematics Series 55, U.S. Government Printing Office, Washington, D.C., 1964.

Bannister, P. R., "Far-Field Extremely Low Frequency (ELF) Propagation Measurements, 1970-1972," *IEEE Trans. Commun.*, Vol. COM-22, No. 4, 1974, pp. 468-474.

Budden, K. G., *Radio Waves in the Ionosphere*, Cambridge University Press, New York, 1961.

Chilton, C. J., D. D. Crombie, and A. G. Jean, "Phase Variation in VLF Propagation," Chap. 19 in *Propagation of Radio Waves at Frequencies Below 300 Kilocycles*, AGARDO Graph 74, Pergamon Press, New York, 1961.

Epstein, P. S., "Reflection of Waves in an Inhomogeneous Absorbing Medium," *Proc. Nat. Acad. Sci., Wash.*, Vol. 16, 1930, p. 627.

Field, E. C., "Propagation of ELF Waves under Normal and Naturally Disturbed Conditions," *J. Geophys. Res.*, Vol. 74, No. 14, 1969, pp. 3639-3650.

-----, "The Effects of Ions on Very Low Frequency Propagation during Polar Cap Absorption Events," *Radio Sci.*, Vol. 5, No. 2, 1970, pp. 591-600.

Field, E. C., and R. G. Joiner, "An Integral-Equation Approach to Long-Wave Propagation in a Non-Stratified Earth-Ionosphere Waveguide," *Radio Sci.*, Vol. 14, No. 6, 1979, pp. 1057-1068.

Galejs, J., *Terrestrial Propagation of Long Electromagnetic Waves*, Pergamon Press, New York, 1972.

Ginsberg, L. H., "Extremely Low Frequency (ELF) Atmospheric Noise Level Statistics for Project Sanguine," *IEEE Trans. Commun.*, Vol. COM-22, No. 4, 1974, pp. 555-561.

Griefinger, C., and P. Griefinger, "Approximate Method for Determining ELF Eigenvalues in the Earth-Ionosphere Waveguide," *Radio Sci.*, Vol. 13, No. 5, 1978, pp. 831-837.

Pappert, R. A., and W. F. Moler, "Propagation Theory and Calculations at Lower Extremely Low Frequencies (ELF)," *IEEE Trans. Commun.*, Vol. COM-22, No. 4, 1974, pp. 438-451.

Reagan, J. B., and T. M. Watt, "Simultaneous Satellite and Radar Studies of the D Region Ionosphere during the Intense Solar Particle Events of August 1972," *J. Geophys. Res.*, Vol. 81, No. 25, 1976, pp. 4579-4596.

Wait, J. R., "On Phase Changes in Very Low Frequency Propagation Induced by an Ionospheric Depression of Finite Extent," *J. Geophys. Res.*, Vol. 69, No. 3, 1964, pp. 441-445.

-----, *Electromagnetic Waves in Stratified Media*, Pergamon Press, New York, 1970.

White, D. P., and D. K. Willim, "Propagation Measurements in the Extremely Low Frequency (ELF) Band," *IEEE Trans. Commun.*, Vol. COM-22, No. 4, 1974, pp. 457-467.

DISTRIBUTION LIST

Department of Defense

Director
Defense Advanced Research Projects Agency
1400 Wilson Boulevard
Arlington, Virginia 22209

Attn:	TIO	1
	STO	1
	NRMO	1

Director
Defense Communications Agency
8th Street and South Courthouse Road
Arlington, Virginia 22204

Attn:	MEECN Office	3

Defense Technical Information Center
Cameron Station
Alexandria, Virginia 22314

Attn:	TC	12

Director
Defense Nuclear Agency
Washington, D.C. 20305

Attn:	STTL	1
	DDST	1
	RAAE	3
	RAEV	1

Joint Chiefs of Staff
Department of Defense
Washington, D.C. 20301

Attn:	J-6	1

Director
National Security Agency
Fort George G. Meade, Maryland 20755

Attn:	Technical Library	2

Under Secretary of Defense (Research and Engineering)
Department of Defense
Washington, D.C. 20301

Attn:	DDS&SS	2

Defense Logistics Agency
DCASMA-Los Angeles
9920 So. La Cienega Boulevard
Inglewood, California 90301

Attn:	DCRL-GLCC(L3)	1
	Ben Miller	

Department of Commerce

U.S. Department of Commerce
Office of Telecommunications
Institute for Telecommunication Sciences
National Telecommunications and Information Administration
Boulder, Colorado 80303
Attn: W. F. Utlaut 2

Department of the Army

Commander/Director
Atmospheric Sciences Laboratory
U.S. Army Electronics Command
White Sands Missile Range, New Mexico 88002
Attn: DRSEL-BL-SY-S 1
F. E. Niles

Director
U.S. Army Ballistic Research Laboratories
Aberdeen Proving Grounds, Maryland 21005
Attn: George E. Keller 1

Commander
U.S. Army Foreign Sciences and Technology Center
220 7th Street, N.E.
Charlottesville, Virginia 22901
Attn: Robert Jones 1

Department of the Navy

Chief of Naval Operations
Department of the Navy
Washington, D.C. 20350
Attn: NOP 985 1
NOP 094H 1

Chief of Naval Research
Department of the Navy
800 North Quincy Street
Arlington, Virginia 22217
Attn: Code 465, R. G. Joiner 1
Code 427, H. Mullaney 1

Commander
Naval Electronic Systems Command
Department of the Navy
Washington, D.C. 20360
Attn: PME-117 1
PME-117T 1
PME-117-21 1
PME 117-21A 1
PME 117-22 1

Dept. of Navy (cont.)

Director
Naval Ocean Systems Center
Electromagnetic Propagation Division
271 Catalina Boulevard
San Diego, California 92152

Attn:	Code 2200, W. F. Moler	1
	Code 2200, John Bickel	1

Director
Naval Research Laboratory
4555 Overlook Avenue, S.W.
Washington, D.C. 20375

Attn:	Code 7700, Timothy P. Coffey	1
	Code 7709, Wahab Ali	1
	Code 7750, John Davis	2
	Code 2627	6

Commander
Naval Surface Weapons Center (White Oak)
Silver Spring, Maryland 20910

Attn:	Technical Library	1

Office of Naval Research Western Regional Office 1
1030 East Green Street
Pasadena, California 91106

Department of the Air Force

Commander
Air Force Geophysical Laboratory, AFSC
L. G. Hanscom Air Force Base, Massachusetts 01731

Attn:	OPR	1
	LKB, W. Swider	1
	LKB, K. Champion	1

Director
Air Force Technical Applications Center
Patrick Air Force Base, Florida 32920

Attn:	TD	1
	HQ 1035th TCHOG/TFS	1

Department of Defense Contractors

General Electric Company
TEMPO--Center for Advanced Studies
816 State Street
Santa Barbara, California 93102

Attn:	Warren S. Knapp	1
	DASIAC	1

Department of Defense Contractors (cont.)

Lockheed Missiles and Space Company
3251 Hanover Street
Palo Alto, California 94304

Attn:	J. B. Reagan	1
	W. Imhof	1
	Martin Walt	1

Mission Research Corporation
735 State Street
Santa Barbara, California 93101

Attn:	M. Scheibe	1
	D. Sowle	1

Pennsylvania State University
Ionospheric Research Laboratory
College of Engineering
318 Electrical Engineering--East Wing
University Park, Pennsylvania 16802

Attn:	John S. Nisbet	1
	Les Hale	1
	A. J. Ferraro	1
	H. S. Lee	1

R & D Associates
4640 Admiralty Way
Marina Del Rey, California 90291

Attn:	R. Lelevier	1
	F. Gilmore	1
	R. Turco	1

The Rand Corporation
1700 Main Street
Santa Monica, California 90406

Attn:	Cullen Crain	1

Professor Chalmers F. Sechrist 1
155 Electrical Engineering Building
University of Illinois
Urbana, Illinois 61801

Stanford Research Institute
333 Ravenswood Avenue
Menlo Park, California 94025

Attn:	Allen M. Peterson	1
	Ray L. Leadabrand	1

Pacific-Sierra Research Corporation
1456 Cloverfield Boulevard
Santa Monica, California 90404

Attn:	E. C. Field, Jr.	1

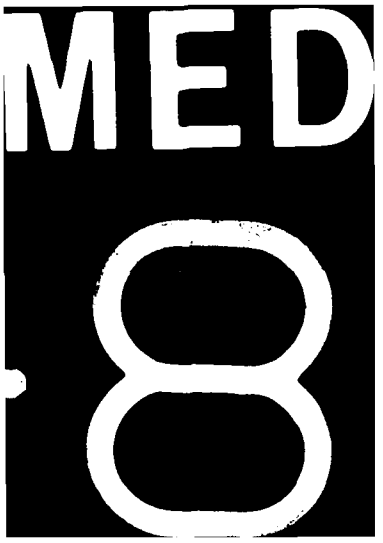
MED
8